ELSEVIER

Chemical Geology 192 (2002) 163–181

CHEMICAL GEOLOGY
INCLUDING
ISOTOPE GEOSCIENCE

www.elsevier.com/locate/chemgeo

The solubility of ruthenium in sulfide liquid: implications for platinum group mineral stability and sulfide melt–silicate melt partitioning

David R.A. Andrews *, James M. Brenan

Department of Geology, University of Toronto, Toronto, Canada M5S 3B1

Accepted 7 March 2002

Abstract

To more completely assess the primary magmatic origin of Ru–Os–Ir (IPGE) alloys, we conducted experiments to evaluate the effects of T, fO_2, fS_2 and melt composition on the solubility of Ru in molten Fe–Ni–sulfide. Fe–Ni–S melt + Ru were held in olivine crucibles, and experiments were done in a vertical-tube gas-mixing furnace at 1200–1400 °C for 1–5 days. At constant fO_2 and fS_2, Ru solubility increases with T, and a similar result is obtained if fO_2 is varied parallel to the fayalite–magnetite–quartz buffer (FMQ), with fS_2 levels to maintain sulfide liquid saturation. At log fS_2 of −1.7, Ru solubility decreases from ~11 wt.% at log fO_2 of −10.8, to ~0.3 wt.% at log fO_2 of −8.1. At a log fO_2 of −8.6, a similar reduction in Ru solubility occurred as log fS_2 decreased from −0.9 to −3.0. Substitution of Ni for Fe in the sulfide results in an increase in Ru solubility, with values ranging from ~3 wt.% at Fe/Ni of 36 to ~10 wt.% at Fe/Ni of 6 (log fO_2, fS_2 of −9.1, −1.7, respectively). Dilution of Ru with a 1:1 mix of Os + Ir results in a 4- and 10-fold decrease in melt Ru content for alloys with ~60 and 35 mol% Ru, respectively. For the fO_2–fS_2 conditions required for sulfide liquid saturation in natural basaltic magmas, pure Ru solubility in molten sulfide is expected to exceed 10 wt.%, and dilution by Os + Ir is still likely to require wt.% levels of Ru for IPGE alloy saturation. Since Ru abundances of ore-grade massive sulfide is <50 ppm, our results would preclude IPGE alloy saturation in the presence of immiscible sulfide liquid. Activity–composition relations determined for Ru in ternary Ru–Os–Ir alloy suggest, however, that the concentration of Ru in molten silicate required for alloy saturation is at or below levels in natural, high Mg igneous rocks, implying such alloys could form in sulfide-undersaturated systems.

The negative fO_2 dependence of Ru solubility in sulfide liquid is opposite that for Ru (and other PGEs) in silicate melt, suggesting that a decrease in fO_2 will favor the partitioning of Ru into the sulfide liquid. However, it is not clear how much this effect will be offset by the concomitant reduction in fS_2 required to maintain saturation in immiscible sulfide liquid. Comparison of our Ru solubility data with values determined in silicate melt yields apparent sulfide–silicate melt partition coefficients that exceed 10^7, which is more than 1000× larger than direct measurements on coexisting sulfide–silicate compositions. Possible reasons for this discrepancy are that (1) measured sulfide–silicate partition coefficients are inaccurate due to incomplete phase separation, (2) non-Henryian activity–composition relations at high Ru concentrations, (3) Ru

* Corresponding author.
E-mail address: andrews@geology.utoronto.ca (D.R.A. Andrews).

PII: S0009-2541(02)00043-8

solubilities in silicate melt measured at both high fO_2 and in the absence of sulfur cannot be accurately extrapolated to the low fO_2 and sulfur-bearing conditions of previous two-liquid partitioning experiments.

Keywords: Solubility of ruthenium; Sulfide liquid; Platinum group mineral stability; Sulfide melt–silicate melt partitioning

1. Introduction

Minerals rich in the elements Os, Ir, and Ru (IPGEs), including laurite (RuS_2), and alloys such as ruthenirridosmine (nomenclature of Harris and Cabri, 1973), have been repeatedly observed as inclusions in chromian spinel and ferromagnesian silicates crystallized in rocks derived from mafic and ultramafic magmas. The list of the occurrences of laurite and IPGE alloys with this paragenesis is extensive (e.g., ophiolites: Prichard et al., 1986; Torres-Ruiz et al., 1996; Edwards, 1990; Legendre and Auge, 1986; layered intrusions: von Gruenewaldt et al., 1989; Maier et al., 1999; Talkington and Lipin, 1986 and references therein), with these phases nearly always being the most abundant platinum group minerals (PGM) present. The common euhedral shape of IPGE mineral inclusions, coupled with the occurrence of chromian spinel, olivine and pyroxene included within IPGE alloy grains (Heazlewood River Complex; Peck et al., 1992), suggests coprecipitation at magmatic conditions. Such observations offer strong textural evidence that laurite and/or IPGE alloy may be an early crystallizing host for the PGEs during solidification of mafic and/or ultramafic magmas (Keays, 1982; Peck et al., 1992). Inasmuch as the predominant PGM composition is rich in the IPGEs, early separation of such alloy phenocrysts offers an effective means to fractionate the IPGE from the PPGE (Rh, Pt, Pd), which is a characteristic feature of mafic/ultramafic lava suites (Barnes and Picard, 1993; Brügmann et al., 1987), as well as cumulate horizons in ophiolites and layered intrusions (Barnes et al., 1985; Maier and Barnes, 1999; Page and Talkington, 1984).

In addition to the textures revealed by natural samples, a first-order assessment of whether IPGE sulfides and alloys are likely to be near-liquidus phases requires information bearing on the solubility of these minerals in mafic and ultramafic melt compositions. While there is scarce data to assess PGM solubilities, direct measurements involving pure metals (e.g., O'Neill et al., 1995; Ertel et al., 1999; Amossé et al., 2000) generally reveal low solubilities at fO_2 relevant to terrestrial magma genesis, although the results of Peach and Mathez (1996) suggest Ir solubilities may be enhanced at high pressure or in the presence of dissolved sulfur. In either case, still lower values may be expected if metal activities are reduced by dilution to form multi-component PGM (Borisov and Palme, 2000). Thus, concentrations required for saturation may approach levels present in mafic/ultramafic rock compositions, although further experimental work is clearly required. The presence of interstitial base-metal sulfide in PGM-bearing cumulate horizons suggests that such rocks were formed from a magma that achieved sulfide-saturation at some point during its crystallization history. The likelihood of IPGE mineral saturation under these conditions is less certain, due to sparse and apparently conflicting data on IPGE solubility in molten sulfide. For example, Fleet and Stone (1991), report solubilities of <1 wt.% Ir and <0.1 wt.% Os in sulfide melt coexisting with Fe–Ir and Os alloys from experiments done at 1 atm and 1200 °C. In contrast, Peach and Mathez (1996) recorded a solubility of ~ 4 wt.% Ir in sulfide melt coexisting with Fe–Ir alloy, from experiments done at 0.8 GPa and 1450 °C. Brenan and Andrews (2001) reported similarly high solubilities for laurite and Ru–Os–Ir alloy at 1 atm and 1200–1300 °C. Thus, although textural evidence suggests that IPGE-rich PGMs could be primary, PGM solubility in molten sulfide could be high enough to preclude PGM crystallisation at sulfide saturation. This would imply that the timing of sulfide liquid immiscibility is crucial if PGMs are to be effective in producing the observed IPGE/PPGE fractionations. Thus, to better interpret the role of IPGE alloys in affecting the PGE geochemistry of mafic/ultramafic magmas, we have conducted a suite of experiments to determine the controls on Ru ($\pm$ Os + Ir) alloy solubility in molten sulfide. Our

experiments focus primarily on ruthenium solubility because this element is a major constituent of the most common IPGE minerals found as inclusions in mafic phenocrysts.

2. Overview of experiments

A complete description of Ru solubility in molten sulfide requires an understanding of the effects of several competing variables. First, in a sulfide melt containing both oxygen and sulfur, Ru will dissolve as both oxide and sulfide species, with solution reactions taking the form:

$$\mathrm{Ru_{solid}} + \frac{x}{4}\mathrm{O_2} \Leftrightarrow \mathrm{RuO_{\frac{x}{2}melt}} \quad (1)$$

$$\mathrm{Ru_{solid}} + \frac{x}{4}S_2 \Leftrightarrow \mathrm{RuS_{\frac{x}{2}melt}} \quad (2)$$

where x is the effective valence of Ru in the melt. Thus, we may anticipate that both oxygen and sulfur fugacities will affect Ru solubility by controlling both the abundance of various melt species, and their activity–composition relations. As such, our experiments were conducted at known fO_2 and fS_2, with values selected to include the range of fO_2 and fS_2 expected for sulfide liquid saturation in magmas with low to moderate FeO contents (Fig. 1). The cation chemistry of the sulfide melt may also have a substantial influence on Ru solubility, as suggested by the results of Brenan and Andrews (2001), who found that increases in melt Fe/Ni caused a reduction in the Ru content of sulfide melt coexisting with laurite + Ru-rich alloy. We have conducted most experiments at an Fe/Ni of ~ 6 (a value typical for massive sulfides), but have also explored Ru solubility over a range of Fe/Ni. Inasmuch as natural PGMs vary from pure Ru to Ru-poor Os–Ir dominated compositions, we have also done experiments to determine how dilution of Ru alloy by Os + Ir will affect solubilities. Finally, the enthalpy change for reactions (1) and (2) are unknown, thus the effect of temperature on Ru solubility cannot be predicted a priori. Consequently, we measured Ru solubilities over the temperature range of 1200–1400 °C, at both fixed fO_2 and fS_2, and have also estimated the temperature effect if fO_2–fS_2 variation is dictated by sulfide liquid saturation. Results of these experiments enable us to explicitly define Ru saturation behavior in sulfide liquids at conditions relevant to natural mafic magmas, thus allowing a more complete assessment of the conditions under which early IPGE alloy crystallization occurs.

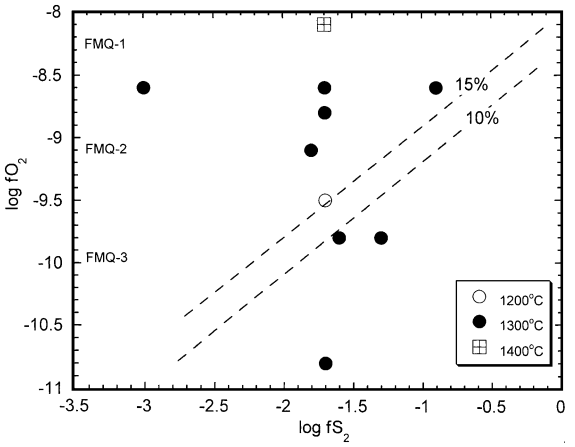

Fig. 1. Comparison of fO_2 and fS_2 investigated in this study with values appropriate for sulfide liquid saturation in natural basaltic magmas having 10 and 15 mol% total FeO (dashed curves) at 1300 °C. The fO_2–fS_2 conditions for sulfide liquid saturation were calculated from the equilibrium constant for the heterogeneous reaction (Wallace and Carmichael, 1992): $1/2O_2 + FeS_{sulf} = 1/2S_2 + FeO_{sil}$. In this case, the activity of FeS in the sulfide melt (FeS_{sulf}) is assumed to be unity, whereas the activity of FeO in the silicate melt at a particular fO_2 (FeO_{sil}) is calculated after the method of Snyder and Carmichael (1992), using melt ferric/ferrous ratios based on the formulation of Kress and Carmichael (1988). Thermodynamic data for FeO and FeS were taken from Robie et al. (1979). Values of fO_2 on the ordinate are labeled in terms of their log deviation from the fayalite–magnetite–quartz buffer (FMQ) at 1300 °C.

3. Experimental technique

Starting materials consisted of metal powders weighed to desired proportions, then thoroughly mixed by grinding under ethanol. Powdered San Carlos (Arizona) olivine (SCO) was added to the metal mixture to prevent the sulfide melt generated in experiments from migrating out of the container. Samples were contained in crucibles fabricated from megacrysts of SCO, which typically held 65–80 mg of the olivine–metal mixture. All experiments were performed using a vertical tube furnace modified for control of fO_2 and fS_2 by gas mixing. For a detailed description of the furnace configuration

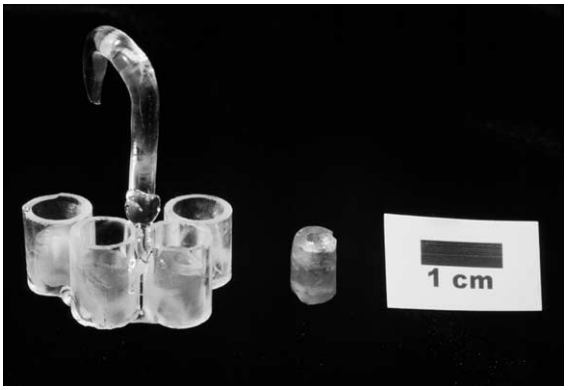

Fig. 2. Photo of sample assembly loaded with three San Carlos olivine crucibles. A single crucible is shown to the right of the assembly; 1 cm scale bar for reference.

see Brenan and Caciagli (2000). Temperatures were monitored with a ceramic sheathed S-type thermocouple, calibrated against the melting point of gold. Specific oxygen and sulfur fugacities were calculated using the 'COSHmix' computer program which uses RAND free energy minimization of data from JANAF thermodynamic tables to calculate the equilibrium speciation of SO_2, CO, and CO_2 at high temperature and one atmosphere pressure. The COSHmix program was supplied courtesy of Dr. Victor Kress. Gas flows were controlled and mixed using a calibrated rotoball flowmeter, and we have checked the accuracy of calculated fugacites using three techniques. We assessed fS_2 using the pyrrhotite sulfur barometer of Toulmin and Barton (1964) at 900 °C and log fS_2 of −1.5, −2 and −3 and bracketed the Ru–RuS_2 equilibrium at 1200 °C. Calculated fO_2 was checked using the stability of solid oxide buffers (nickel–nickel oxide, molybdenum–molybdenum oxide, iron–wüstite), and we have also employed the NiO–Pd redox sensor at 1000 °C (Pownceby and O'Neill, 1994). Using these techniques, we estimate fS_2 and fO_2 accuracy to be within 0.3 log units.

Table 1
Summary of experiment conditions

Experiment	Duration (h)	Temperature (°C)	log fO_2	log fS_2	Gas flow rates (ccm) CO–CO_2–SO_2
Ru282c	48	1300	−8.1	−1.7	25–80–30
Ru192	24	1300	−8.8	−1.7	34.8–64.5–8.7
Ru392	75.5	1300	−8.8	−1.7	34.8–64.5–8.7
Ru592	120	1300	−8.8	−1.7	34.8–64.5–8.7
Ru3112_rev_92	24	1300	−8.8	−1.7	34.8–64.5–8.7
Ru392Fe	71	1300	−9.1	−1.8	55.2–81.4–8.0
Ru392Fe_b	71	1300	−9.1	−1.8	55.2–81.4–8.0
Ru392Fe_e	72	1300	−9.1	−1.8	55.2–81.4–8.0
Ru3102	76	1300	−9.8	−1.6	42.5–21.6–4.5
Ru3112c	48	1300	−10.8	−1.7	50–7–2.7
Ru2112c_rev_82	48	1300	−8.1	−1.7	25–80–30
Ru391[2]	72	1300	−8.6	−0.9	27–0–15.9
Ru292s	48	1300	−8.6	−1.7	30–70–11
Ru393	72	1300	−8.6	−3.0	65–237.2–4.7
Ru2101	48	1300	−9.8	−1.0	27.6–0–6.6
Ru3102Nia_1200	71	1200	−9.5	−1.7	43.9–128.1–15.4
Ru3102Nib_1200[2]	71	1200	−9.5	−1.7	43.9–128.1–15.4
Ru3102_1200	71	1200	−9.5	−1.7	43.9–128.1–15.4
Ru2102_1200t	48	1200	−9.8	−1.6	18–40–5
Ru282_1400	48	1400	−8.1	−1.7	10.5–12–2
RuOsIr3102A	68	1300	−9.8	−1.6	42.5–21.6–4.5
RuOsIr3102B	68	1300	−9.8	−1.6	42.5–21.6–4.5

(1) Experiments with RuOsIr were doped with equal amounts of Os and Ir, all others contained Ru as sole PGE additive.
(2) Experiment was not saturated in alloy phase.
(3) Experiment labels are read as follows: PGE added, duration in days, −log fO_2, −log fS_2 (rounded to nearest integer), i.e. Ru3112_rev_92 had only Ru, was run for 3 days at log fO_2 = −10.8, log fS_2 = −1.6 and was then reversed at log fO_2 = −8.8, log fS_2 = −1.7.

Holders for the olivine crucibles were fabricated from silica rod and cylinders cut from silica tubing, and up to four SCO crucibles could be run in this configuration (Fig. 2). Sample holders were suspended from a hook fashioned at the end of a ~ 60 cm length of 3 mm diameter silica rod. In a typical experiment, the silica rod was retracted so that the loaded sample holder was initially positioned in the upper cool region of the furnace. The furnace was then sealed and gas flow commenced. After 20–30 min, the rod was lowered to position the holder within the predetermined furnace hot spot, where samples remained for 1–5 days. Samples were quenched by rapid immersion in a cold water bath. A full list of all experiments conducted in this study is provided in Table 1.

4. Analytical methods

Run products were mounted in epoxy and sectioned using a diamond saw to expose a cross-section of the olivine crucible. Sectioned samples were prepared for electron microprobe analysis by hand grinding with SiC paper and polishing with 1 and 0.3 μm diamond paste, then colloidal silica. Phase compositions were obtained using the Cameca SX 50 electron microprobe at the University of Toronto using a 20-kV accelerating voltage. IPGE alloys were analyzed using a 60-nA focused beam, with 20 s count times on each X-ray peak. Sulfide melt analysis utilized a 100-nA beam current, counting 10 s on peak for Fe, Ni, and S, 20 s on peak for oxygen and 60 s on peak for Ru, Os, and Ir. Most melt compositions were determined by broad beam analysis, in which the electron beam diameter was increased to 10 μm to compensate for any textural (and hence chemical) inhomogeneity produced by quench crystallization. Two experiments (Ru3112c and Ru2101) contained abundant, coarse Ru metal as a quench phase (see below), making it impossible to determine melt compositions even by broad beam analysis. For those experiments, we analyzed individual quench phases using a focused beam, and combined this data with the modal abundance of each phase (determined by

Table 2
Results of electron microprobe analysis of sulfide liquid (wt.% element)

Experiment I.D	*n*	Fe	Ni	S	Ru	O	Os	Ir	Total	Fe/Ni
Ru282c	11	53.38(2.21)	13.86(3.03)	28.65(1.47)	0.30(0.15)	3.61(1.22)			99.81	3.85(0.86)
Ru192	13	55.64(1.60)	8.13(1.96)	29.13(0.47)	2.73(0.93)	4.97(1.00)			100.59	6.85(1.67)
Ru392	15	55.44(2.54)	8.37(2.05)	28.85(1.11)	2.86(1.07)	4.42(1.47)			99.93	6.62(1.65)
Ru592	16	55.41(1.36)	9.09(1.71)	29.10(0.58)	2.57(0.57)	4.02(0.95)			100.18	6.09(1.16)
Ru3112b_rev_92	5	52.89(2.12)	9.40(3.35)	30.33(1.35)	3.08(1.04)	4.04(2.47)			99.75	5.63(2.02)
Ru392Fe	17	46.80(0.94)	7.98(0.38)	32.48(0.82)	11.08(1.12)	0.17(0.40)			98.51	5.86(0.30)
Ru392Fe_b	20	53.91(1.00)	4.17(0.24)	32.61(0.62)	7.06(1.16)	0.90(0.73)			98.65	12.93(0.79)
Ru392Fe_e	17	61.35(0.72)	1.73(0.09)	30.56(0.94)	2.62(0.53)	3.36(0.86)			99.68	35.52(1.85)
Ru3102	15	44.29(2.45)	7.73(0.49)	32.82(0.98)	14.25(2.75)	0.57(1.27)			99.66	5.73(0.48)
Ru3112c[2]	7	51.70(1.06)	6.20(0.40)	33.40(0.97)	10.19(1.82)	0.00(0.00)			101.49	8.34(0.56)
Ru2112c_rev_82	9	51.78(3.48)	13.92(4.14)	29.00(1.53)	0.61(0.18)	2.76(0.93)			98.07	3.72(1.20)
Ru391	7	41.51(2.91)	7.73(0.59)	30.64(0.56)	17.37(3.73)	1.52(0.72)			98.80	5.37(0.56)
Ru292s	16	55.96(2.13)	10.41(2.36)	28.11(0.93)	0.65(0.33)	4.95(1.25)			100.07	5.38(1.24)
Ru393	13	60.77(5.14)	6.84(5.57)	27.42(1.41)	0.28(0.14)	5.26(1.68)			100.56	8.89(7.28)
Ru2101[2]	14	24.08(2.53)	4.53(0.23)	27.62(0.30)	44.48(2.95)	0.00(0.00)			100.70	5.32(0.62)
Ru3102Nia_1200	10	49.65(2.09)	14.67(2.63)	28.75(0.98)	3.74(1.08)	4.01(1.32)			100.82	3.38(0.62)
Ru3102Nib_1200	14	34.36(1.71)	22.00(3.23)	31.33(0.50)	11.87(2.86)	0.58(0.69)			100.14	1.56(0.24)
Ru3102_1200	4	55.03(1.89)	6.93(1.25)	29.47(1.02)	3.01(0.63)	7.11(0.74)			101.56	7.94(1.46)
Ru2102_1200t	13	53.32(2.33)	9.48(2.59)	30.43(0.66)	3.85(0.84)	3.20(1.20)			100.28	5.62(1.56)
Ru282_1400	7	49.54(3.57)	17.29(3.30)	27.67(1.87)	0.37(0.17)	3.31(1.36)			98.18	2.87(0.58)
RuOsIr3102A	20	54.09(1.03)	8.05(0.98)	32.32(0.69)	3.57(1.03)	1.08(0.69)	0.02(0.02)	0.06(0.09)	99.19	6.45(0.49)
RuOsIr3102B	13	54.31(0.78)	9.47(1.08)	32.17(0.98)	1.65(0.32)	1.18(0.85)	0.09(0.11)	0.17(0.20)	99.04	6.00(0.55)

(1) Number in parenthesis is one standard deviation based on *n* analyses.
(2) Melt composition calculated using focused-beam analyses of quench sulfide and Ru dendrites combined with modal abundances.

Table 3
Results of electron microprobe analysis of IPGE phenocrysts (wt.% element)

Experiment	*n*	Fe	Ni	S	Ru	Os	Ir	Total
Ru282c	9	1.57(0.18)	0.51(0.03)	0	98.50(0.46)			100.57
Ru192	10	1.54(0.30)	0.24(0.18)	0	98.82(0.50)			100.60
Ru392	20	1.51(0.33)	0.23(0.20)	0	98.74(0.59)			100.51
Ru592	10	1.29(0.10)	0.12(0.02)	0	98.84(0.29)			100.24
Ru3112_rev_92	15	1.36(0.18)	0.14(0.04)	0	98.31(0.24)			99.82
Ru392Fe	10	1.31(0.08)	0.10(0.01)	0	99.18(0.55)			100.43
Ru392Fe_b	7	1.36(0.06)	0.04(0.01)	0	99.07(0.25)			100.34
Ru392Fe_e	20	1.57(0.08)	0.04(0.01)	0	99.31(0.32)			100.42
Ru3102	10	1.23(0.05)	0.07(0.01)	0	99.25(0.63)			100.55
Ru3112c	11	2.20(0.09)	0.14(0.02)	0	98.27(0.75)			100.61
Ru2112c_rev_82	11	1.63(0.62)	0.11(0.04)	0	98.05(0.77)			99.80
Ru391[2]	n/a							
Ru292s	15	1.73(0.12)	0.38(0.11)	0	98.95(0.43)			101.06
Ru393	10	3.31(0.21)	0.83(0.17)	0	96.51(0.50)			100.43
Ru2101	19	0.68(0.02)	0.05(0.02)	0	99.77(0.37)			100.50
Ru3102Nia_1200	10	0.87(0.16)	0.18(0.05)	0	99.16(0.45)			100.21
Ru3102Nib_1200[2]	n/a							
Ru3102_1200	6	0.97(0.14)	0.14(0.03)	0	99.59(0.26)			100.73
Ru2102_1200t	8	1.14(0.14)	0.15(0.02)	0	99.59(0.29)			100.88
Ru282_1400	10	2.72(0.21)	0.65(0.09)	0	97.41(0.44)			100.78
RuOsIr3102A	20	2.16(0.27)	0.13(0.03)	0	45.90(0.82)	25.36(0.95)	28.36(0.72)	101.92
RuOsIr3102B	20	3.11(0.31)	0.22(0.05)	0	25.36(0.54)	33.37(2.33)	39.68(1.78)	101.75

(1) Number in parentheses is one standard deviation based on *n* analyses.
(2) Run product was not alloy saturated.

image processing) to calculate melt compositions. X-ray lines used to determine element concentrations were: Fe (kα), Ni (kα), S (kα), O (kα), Ru (Lα), Os (Lα), Ir (Lα). Pentlandite was used as a standard for Fe, Ni, and S, hematite for O, and pure metals for the IPGEs. Oxygen was analysed using an ODPB pseudocrystal, and the hematite standard was carbon-coated at the same time as the unknowns to minimize inaccuracies due to the effects of coat thickness on oxygen X-ray attenuation. Summaries of sulfide and alloy compositions are provided in Tables 2 and 3, respectively.

5. Results

5.1. Textural observations

Polished sections of experiments reveal subhedral phenocrysts of olivine along with IPGE alloy, the latter phase exhibiting one of two growth habits. In most cases, alloys are subhedral to euhedral, and display hexagonal cross-sections, with a tabular morphology (Fig. 3b–d). Alloys that exhibit this morphology are considered to have been stable phenocrysts during a particular experiment. In contrast, experiments done at the highest fS_2 (Ru391) and lowest Fe/Ni (Ru3102Nib_1200), contained alloys exhibiting a dendritic habit (Fig. 3a), suggesting crystallization upon quenching of the sample. In those instances, stable alloy is inferred to have not been present during an experiment, and reported solubilities represent minimum values. In one instance (experiment Ru2101; Fig. 3c), skeletal laurite is intergrown with metal dendrites, suggesting this phase also crystallized on quench.

Alloy phenocrysts showed systematic changes in morphology with changes in oxygen fugacity. With a decrease in fO_2 from $10^{-8.1}$ to $10^{-9.8}$ atm, crystal shape varied from rounded to subhedral to euhedral, with progressive development of hexagonal cross-sections. Over the same range of conditions, the crystal number density decreased, while phenocryst grain size increased. In experiments where Os and Ir were added to the starting materi-

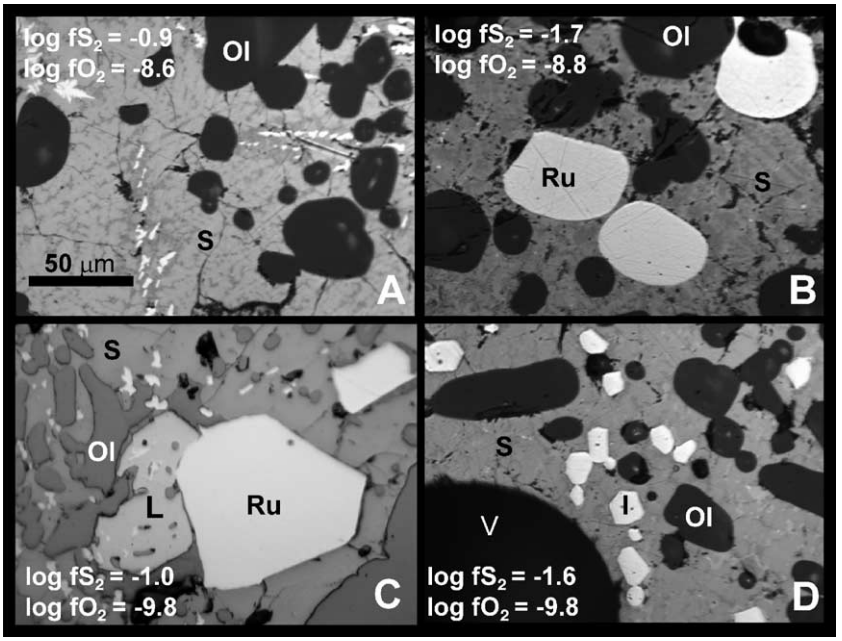

Fig. 3. Reflected light photomicrographs (plane polarized light) of sectioned and polished run-products (S = sulfide melt, Ru = Ruthenium phenocrysts, L = Laurite, Ol = Olivine, I = RuOsIr alloy, V = vesicle); (A) Ru391 (note the Ru dendrites, a product of quench crystallization), (B) Ru392, (C) Ru2101 (note the skeletal texture of the laurite, which is intergrown with quench dendrites of Ru), (D) RuOsIr3102A (alloys in this experiment are ~ 60% Ru, 40% [Os + Ir]).

als, alloy phenocrysts exhibited a euhedral morphology, with a distinctly smaller grain size and high number density.

5.2. Attainment of equilibrium

We have assessed the approach to equilibrium in our experiments in several different ways. First, we conducted a series of experiments, all at 1300 °C using identical starting materials, run for durations of 1, 3 and 5 days (Ru192, Ru392 and Ru592; Table 1) and found that Ru solubilities were identical (Fig. 4), indicating rapid Ru solution into the sulfide liquid. This result is in contrast to that of Peach and Mathez (1996), who observed a progressive increase in melt Ir content as a function of run duration in experiments done at 1450 °C and 0.8 GPa. Inasmuch as these workers relied on internal buffering, and the assumption of vapor saturation to fix fO_2 and fS_2, it is possible that the time evolution in metal solubility seen in their experiments is a product of progressive changes in sample fO_2 (or fS_2), possibly coupled to vapour loss. Alternatively, it may be that Ir metal dissolves more slowly in sulfide melt at their experimental conditions, although our own 1 atm reconnaissance

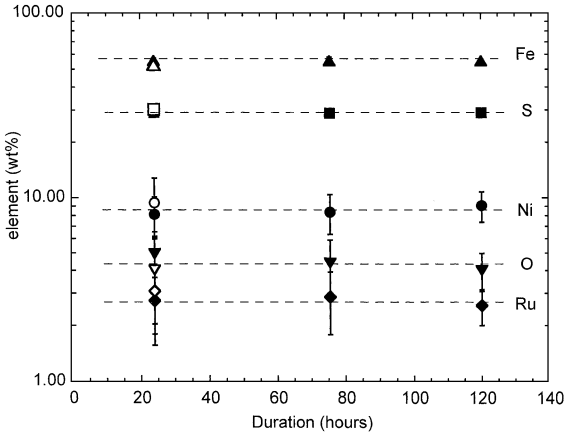

Fig. 4. Sulfide melt compositions from experiments Ru392, Ru192 and Ru592 as a function of run duration (solid symbols). Open symbols are for reversal experiment Ru3112rev_92.

experiments have shown Ir solution to be as rapid as Ru. In addition to time invariance of Ru solubility, we were also able to "reverse" our solubility measurements. This was accomplished by running pairs of samples initially at conditions in which the Ru solubility is high (~ 11 wt.% at log $fO_2 = -10.8$, log $fS_2 = -1.7$), then, upon quenching, one crucible was retained for EMP analysis while the other was re-run at conditions in which the Ru solubility is lower. We did this procedure for two different sets of conditions in the second step (log $fO_2 = -8.1$ and -8.8, both at log $fS_2 = -1.7$) and found that solubilities are within error of equivalent forward experiments. In addition to these more direct tests for chemical equilibrium, we also did multiple electron microprobe analyses across the largest (30 + microns) of the alloy phenocrysts produced in experiments, and found them to be compositionally homogeneous. This homogeneity is also reflected in the low standard deviation in alloy analyses provided in Table 3.

5.3. IPGE phenocryst compositions

In experiments with Ru as the sole IPGE, alloy phenocrysts contained 2–8 mol% Fe + Ni (most commonly 4 mol%), with the remainder being ruthenium. Whereas the relative concentration of Fe and Ni in the phenocrysts varied systematically with each of the parameters explored in this study, Ru concentrations remained essentially constant. Thus, the activity of Ru is nearly the same in experiments, and close to unity. At fixed fS_2 and melt composition, decreasing oxygen fugacity ($10^{-8.1}$ to $10^{-9.8}$ atm) caused Fe concentrations in the alloy to slightly increase (~ 0.5 mol%) while the molar abundance of Ni decreased by an equivalent amount. A decrease in fS_2 from $10^{-1.7}$–$10^{-3.0}$ atm resulted in an ~ 4 mol% decrease in Ru concentration, which was balanced by a ~ 3 and 1 mol% increase in Fe and Ni concentrations, respectively. As expected, alloys produced in experiments in which Fe in the sulfide melt were replaced by Ni showed a corresponding increase in their Fe/Ni ratio. The composition of alloys produced in experiments with added Os + Ir is portrayed in Fig. 5. As shown, the series of compositions produced span the range of Ru contents for natural IPGE alloys, and are intermediate in their Os/Ir ratio. The addition of Os and Ir to the alloy resulted in considerably more uptake of Fe and Ni (Table 3), which is consistent with the reduced activity coefficients for Fe (and probably Ni) in Os and Ir relative to Ru alloys (e.g. Borisov and Palme, 2000). At constant fO_2, fS_2 and melt Fe/Ni, the Fe and Ni contents of Ru alloys decrease with decreasing temperature.

5.4. Sulfide melt compositions

Ruthenium solubilities were found to change markedly as a function of all of the parameters we explored, with values ranging from ~ 0.3 to 44 wt.%. The effects of each parameter are described separately below.

5.4.1. Effect of fO_2

Analysis of the sulfide melt from experiments in which oxygen fugacity was varied from $10^{-8.1}$ to $10^{-10.8}$ atm at a constant fS_2 of $10^{-1.7}$ atm (Fig. 6a) revealed that Ru concentrations increase in a non-linear manner from 0.3 wt.% at $fO_2 = 10^{-8.1}$ to ~ 12 wt.% at fO_2 values greater than 10^{-9} atm. The Ru solubility changes abruptly over a narrow fO_2 interval between $10^{-8.8}$ and $10^{-9.1}$ atm. In concert with these changes in Ru solubility, the oxygen content of sulfide liquids decreased from ~ 4 wt.% at $fO_2 = 10^{-8.1}$ atm to undetectable levels at $fO_2 = 10^{-10.8}$ atm, with a complimentary increase in S abundance from ~ 27 to 32 wt.%. Consideration of the effect of fO_2 on reaction (1) would suggest that increasing fO_2 would promote solution of Ru if this element is dissolving as an oxide species. The observed *negative* correlation between fO_2 and Ru solubility, however, suggests that Ru does not dissolve in this manner, in contrast to its solution behavior in silicate melts (e.g. Borisov and Nachtweyh, 1998). Indeed, it would appear that addition of oxygen to the sulfide melt markedly raises the activity coefficients for Ru melt species.

5.4.2. Effect of fS_2

The effect of sulfur fugacity on Ru solubility was investigated at oxygen fugacities of $10^{-8.6}$ and $10^{-9.8}$atm, and in both cases, Ru solubility increased sympathetically with fS_2 (Fig. 6b). At an

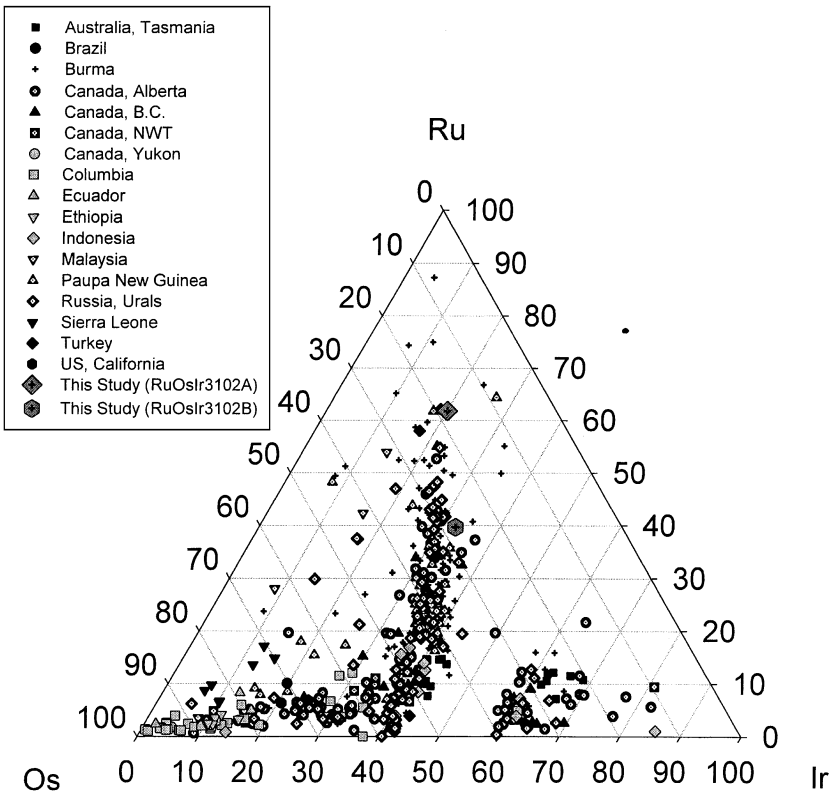

Fig. 5. Ternary diagram depicting the composition (at.%) of RuOsIr alloys produced in our experiments along with alloys from various natural parageneses. Data from Cabri et al. (1996).

fO_2 of $10^{-8.6}$ atm, values range from 0.3 wt.% at fS_2 of $10^{-3.0}$ atm to >16 wt.% at fS_2 of $10^{-0.9}$atm. At fO_2 of $10^{-9.8}$ atm, solubilities were systematically higher, with values increasing from ~ 12 to 44 wt.% as fS_2 increased from $10^{-1.6}$ to $10^{-1.0}$ atm. Not surprisingly, the observed variation in Ru solubility with fS_2 is consistent with behavior described by reaction (2), indicating Ru solution as sulfide species.

5.4.3. Effect of melt composition

Two series of experiments were conducted to investigate the effect of sulfide melt Fe/Ni ratio on Ru solubility. Three experiments were done at fO_2 of $10^{-9.1}$ atm, fS_2 of $10^{-1.8}$ atm and 1300 °C and three at $fO_2 = 10^{-9.5}$ atm, $fS_2 = 10^{-1.7}$ atm and 1200 °C. In both series, Ru concentrations in alloy-saturated melt decreased with an increase in Fe/Ni (Fig. 6c), consistent with the previous laurite solubility measurements of Brenan and Andrews (2001). Correlated with the overall decrease in Ru solubility with increasing Fe/Ni is an overall increase in melt oxygen content. At constant fO_2, it appears that higher Fe melts contain more oxygen, behavior that was also noted by Rose and Brenan (2001) in experiments in which Fe in the sulfide melt was substituted by Co, Ni or Cu. The implication of this result is that at a given fO_2, solution of Fe in sulfide melt involves a greater association with oxygen than is the case for other transition metals. A similar correlation between oxygen concentration and Ru solubility was noted above for experiments run at constant Fe/Ni, but variable fO_2. The Ru–oxygen relations for both sets of experiments are portrayed in Fig. 6d. The trend in Ru solubility with melt oxygen content is similar, regardless if oxygen varies by changes in fO_2, or Fe/Ni, suggesting that it may not be the identity of the cation as much as the

addition of O with Fe that affects the activity coefficients of Ru species in the melt.

5.4.4. Effect of adding Os and Ir

In experiments done at fO_2 of $10^{-9.8}$ atm, fS_2 of $10^{-1.6}$ atm and 1300 °C, the solubility of ruthenium in the sulfide melt showed a marked decrease as the coexisting alloy was diluted by Os + Ir (Fig. 6e). Specifically, the solubility of pure Ru at these conditions is ~ 15 wt.%, whereas values dropped to 3.6 and 1.7 wt.% as the mole fraction of Ru in the alloy (X_{Ru}) decreased to ~ 0.58 and ~ 0.36, respectively.

5.4.5. Effect of temperature

We assessed the effect of temperature on Ru solubility by conducting experiments at fO_2 of

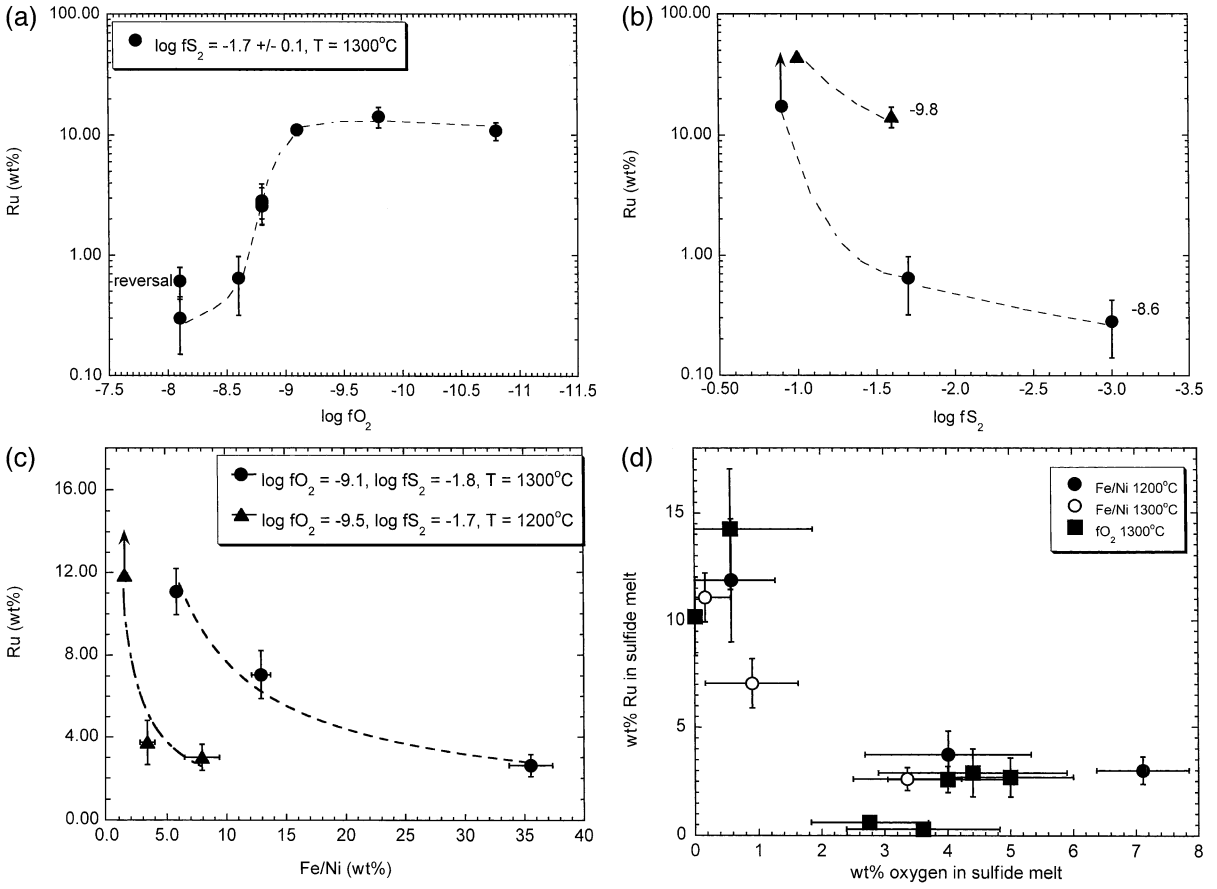

Fig. 6. (a) Variation in melt Ru concentration as a function of log fO_2 for experiments at 1300 °C and log $fS_2 = -1.7$. Data point labeled reversal is experiment Ru2112_rev_82, first run for 2 days at log $fO_2 = -10.8$ and re-run at log $fO_2 = -8.1$. (b) Variation in melt Ru concentration (wt.%) as a function of log fS_2 for experiments at 1300 °C and log $fO_2 = -9.8$ and -8.6. For each oxygen fugacity Ru concentration increases with increasing sulphur fugacity. (c) Variation in melt Ru concentration as a function of melt Fe/Ni ratio for experiments done at 1300 °C, log $fO_2 = -9.1$ and log $fS_2 = -1.8$ and 1200 °C, log $fO_2 = -9.5$ and log $fS_2 = -1.7$. (d) Variation in melt Ru concentration as a function of melt oxygen content for experiments done at both variable Fe/Ni ratio and fO_2. (e) Variation in melt Ru concentration as a function of Ru content of coexisting RuOsIr alloy for experiments done at 1300 °C, log $fO_2 = -9.8$ and log $fS_2 = -1.6$. (f) Variation in melt Ru concentration as a function of temperature for experiments done at log fO_2 of -8.1 and -9.8 and log $fS_2 = -1.7$. (g) Comparison of fO_2–fS_2 conditions required for sulfide liquid saturation in a silicate melt with 31 mol% total FeO at 1200 and 1300 °C (see caption to Fig. 1 for details of calculation). Dashed curves are isopleths of ΔFMQ. Also shown is the fO_2 and fS_2 conditions for experiment Ru3102_1200t, which was run at FMQ -1.5. To maintain sulfide liquid saturation with increasing temperature and constant ΔFMQ requires the fS_2 to increase along the isopleth labeled "-1.5".

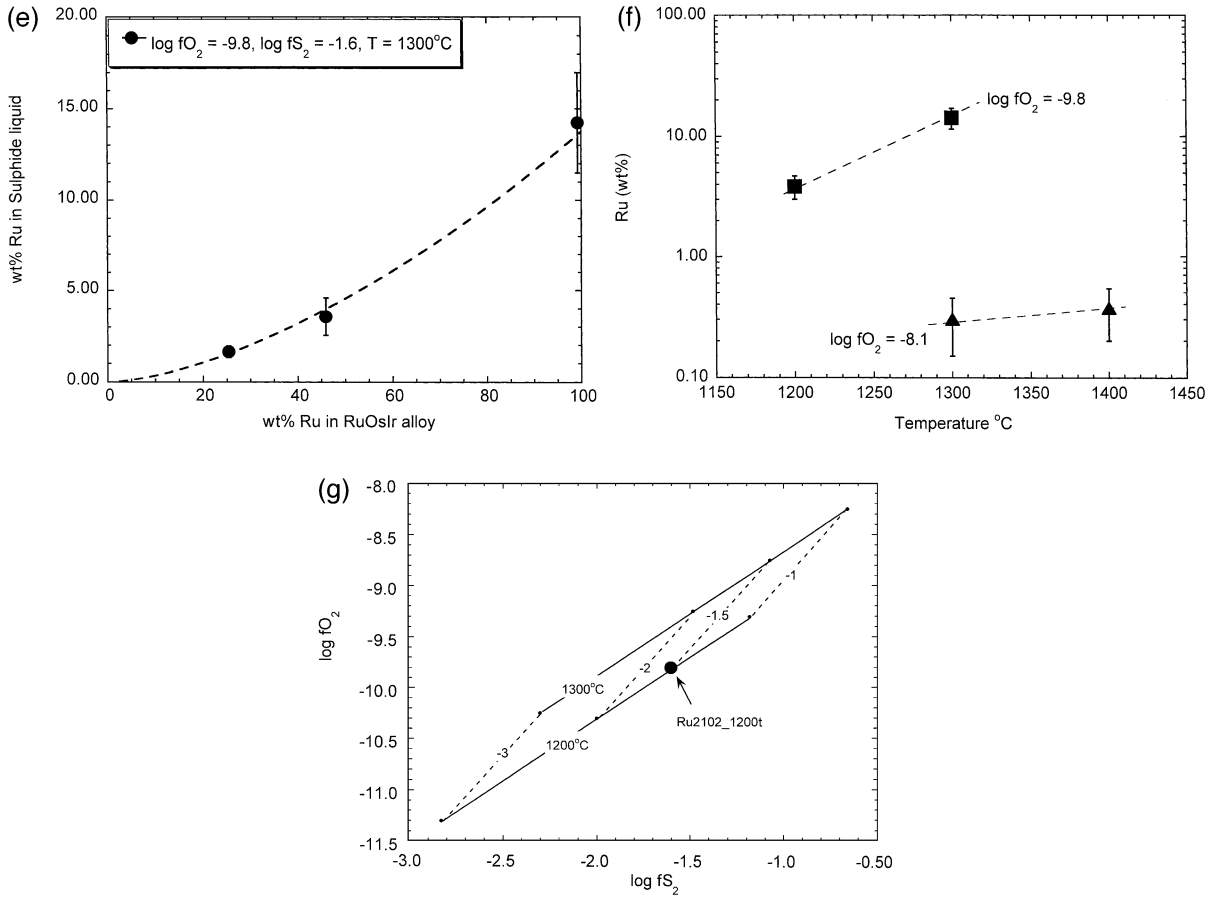

Fig. 6 (*continued*).

$10^{-9.8}$ and $10^{-8.1}$ atm, and fixed fS_2 of $10^{-1.7}$ atm. Results are portrayed in Fig. 6f, and show that, at each fO_2, the solubility decreases with decreasing temperature, although the T effect at log fO_2 of -8.1 is smaller than at log fO_2 of -9.8. To maintain saturation in a sulfide liquid, however, the fO_2 and fS_2 of a natural magma cannot remain constant with changes in temperature, and an accurate assessment of the temperature dependence on Ru solubility should account for these effects. Fig. 6g shows the fO_2–fS_2 conditions for sulfide saturation at 1200 and 1300 °C in a silicate magma with 31 mol% total FeO (although this melt iron content is high for a natural basaltic magma, it is appropriate for sulfide liquid saturation at the conditions for experiment Ru2102_1200t, and serves the purpose of illustration). Inasmuch as the fO_2 of natural magmas track parallel to the common solid oxide buffers (Carmichael, 1991), we have portrayed the T dependence of the fO_2–fS_2 trajectory for a sulfide-saturated magma assuming that fO_2 tracks parallel to the fayalite–magnetite–quartz (FMQ) buffer. As shown, at constant relative fO_2, the fS_2 required for sulfide saturation increases with increasing temperature. For the case of the experiment done at 1200 °C (Ru2102_1200t), to maintain sulfide liquid saturation from 1200 to 1300 °C, at a constant relative fO_2 of FMQ -1.5, requires the fO_2 to increase from $10^{-9.8}$ to $10^{-8.8}$ atm, and the fS_2 to increase from $10^{-1.6}$ to $10^{-1.1}$ atm. Although we did not do an experiment at the precise conditions for saturation at 1300 °C, interpolation of the 1300 °C solubility data for fO_2 of $10^{-8.8}$ atm (Fig. 6b) yields a solubility of $\sim$ 15 wt.% at fS_2 of $10^{-1.1}$ atm. Thus, the "realistic" effect of temperature accounted for in

this manner yields a change in solubility that is very similar to the effect seen if both fO_2 and fS_2 are held constant.

6. Discussion

6.1. Solubility of other IPGE-bearing phases

Fleet and Stone (1991) report results from experiments at 1 bar and 1200 °C that produced sulfide melt with <1 wt.% Ir and <0.1 wt.% Os coexisting with alloys containing 77–88 wt.% Ir and 97 wt.% Os. Similarly low Ir and Os concentrations were measured by Brenan and Andrews (2001) for sulfide melt coexisting with Ru–Os–Ir alloy at 1200–1300 °C, fS_2 of 10^{-1}–10^{-2} atm and fO_2 10^{-8}–10^{-10} atm. These values are generally consistent with the low Os and Ir contents of sulfide melt produced in our Ru–Os–Ir alloy-saturated experiments, although our alloys contained less Os and Ir than those produced by these latter workers. Such results show that the Os and Ir content of sulfide melt required for alloy saturation is much lower than for Ru, presenting the possibility that some of the near-endmember Os and Ir alloys reported in natural parageneses (see Fig. 5), could be stable in the presence of sulfide liquid. Regardless of how low melt Os and Ir contents are, high Ru-levels in the melt are nonetheless required to stabilize Ru-bearing ternary alloy compositions. In contrast to the much lower Ir solubilities inferred from the aforementioned experiments, Peach and Mathez (1996) measured relatively high Ir concentrations (~ 4 wt.%) in sulfide melt equilibrated with Ir–Fe alloy (~ 90% Ir) at 0.8 GPa and 1450 °C. Such a high Ir solubility may reflect the higher temperature of those experiments, as values are likely to increase with temperature, based on our assessment for Ru. Pressure may also serve to increase Ir alloy solubility in sulfide melt, although we are unaware of any experiments that have systematically documented this effect.

6.2. Implications for alloy and laurite stability during melting and solidification

The results of our assessment of the effects of fO_2, fS_2, melt Fe/Ni, alloy composition and temperature are sufficiently complete to allow us to determine the likelihood of IPGE alloy saturation under sulfide saturated conditions in natural magmas. Using the trends in Ru solubility with fO_2 and fS_2, we have calculated solubilities for the fO_2–fS_2 conditions of sulfide liquid saturation at 1300 °C, for a silicate melt containing 15 mol% (~ 18 wt.%) FeO, which is at the high end of concentrations in tholeiitic magmas. Results (Fig. 7) are portrayed in terms of Ru solubility as a function of fO_2, in which values of fO_2 correspond to a particular fS_2 to maintain sulfide liquid saturation. Also shown are the Ru contents of sulfide liquid required to saturate in Ru–Os–Ir alloy (Os/Ir = 1) with 58 and 36 mol% Ru. These curves were calculated by assuming that the relative reduction in Ru solubility shown in Fig. 6e applies to the range of fO_2 and fS_2 portrayed.

For a given alloy composition, the Ru solubility changes little over a large range of fO_2, mainly because the reduction in alloy solubility that accompanies an fO_2 increase is balanced by the increase in solubility that follows the rise in fS_2 required to maintain sulfide liquid saturation. Over a broad range of X_{Ru} in the alloy, the Ru content of the sulfide liquid

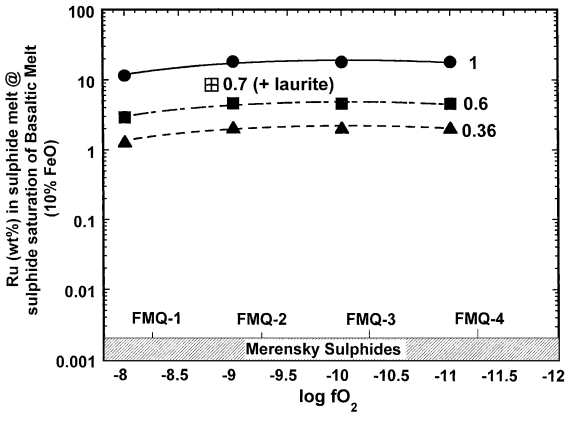

Fig. 7. Estimated Ru solubility in a sulfide melt at 1300 °C as a function of oxygen fugacity. All curves are plotted at fO_2 and fS_2 conditions appropriate for sulfide saturation in a basaltic melt (FeO = 15 mol%). Curves are labeled for the mole fraction of Ru in the alloy phase. The single point labeled $X_{Ru} = 0.7$ corresponds to experiment fRu5 of Brenan and Andrews (2001) run at 1250 °C that was saturated in both laurite and Ru–Os–Ir alloy. For comparison is shown the upper range of Ru contents from sulfides in the Merensky Reef of the Bushveld Complex (data from Naldrett, 1981).

required to maintain saturation is at wt.% levels, and it should be noted here that for melts with lower total FeO contents, the fS_2 required for saturation in sulfide liquid is higher, and therefore Ru solubilities will also be higher. We have also included the results of experiment fRu5 from Brenan and Andrews (2001), which was run at similar conditions to the experiments of this study, but at 1250 °C, and was subsequently saturated in both Ru–Os–Ir alloy ($X_{Ru}=0.7$) and laurite. The Ru content of the sulfide melt required for alloy–laurite saturation is also high (~ 8 wt.%), and consistent with the variation in solubility with alloy composition determined in this study. In addition to the solubility relations, Fig. 7 also depicts the maximum Ru content of ore-grade sulfide liquid segregations associated with mafic and ultramafic intrusive and extrusive rocks. The PGE levels in such rocks are higher than is typical for immiscible sulfide globules in mafic lavas, and thus serves to provide a robust test of whether sulfide-saturated magmas are likely to crystallize IPGE alloys. As the Ru concentrations of these sulfide liquid segregations are at the ppm level, they clearly fall below the saturation levels required by our experiments, indicating that IPGE alloy crystallization is unlikely once a mafic magma achieves sulfide liquid saturation. Both Peach and Mathez (1996) and Brenan and Andrews (2001) came to similar conclusions, based on their finding of wt.% solubility levels for other IPGE-bearing phases (Ir alloy and laurite; discussed above), albeit over a more restricted range of experimental conditions.

Given the conclusion that IPGE alloys (or laurite) are unlikely to crystallize in sulfide saturated mafic magmas, the occurrence of these phases as inclusions in primary ferromagnesian phenocrysts, which are in turn in contact with matrix base metal sulfides, would seem paradoxical. Accepting the preserved textural relations as indicating early crystallization of the included PGMs requires, however, that interstitial sulfide was introduced after alloy precipitation and subsequent isolation in host phenocrysts. Any alloys that were not initially trapped and thus ''shielded'' from later-forming sulfide liquid would be redissolved, thus accounting for the paucity of laurite or IPGE alloy in the matrix (e.g. Western Bushveld Complex, Maier et al., 1999;Merkle, 1992; Shetland, Prichard et al., 1986). The occasional occurrence of base metal sulfides included with IPGE phases (Zambales Ophiolite, Bacuta et al., 1990; Western Bushveld Complex, Maier et al., 1999) would therefore be a consequence of the grain boundary mobility that accompanies post-solidification compaction and annealing. Rose and Brenan (2001) and Brenan and Rose (in press) have shown that at fO_2 that exceeds FMQ-1.6, chromite, as well as ferromagnesian silicates like olivine, will be readily wetted by sulfide liquid, making them susceptible to infiltration to achieve surface energy reduction (e.g., Watson, 1981). Thus, later-formed sulfide melt could readily permeate pre-existing cumulates, thus precipitating the observed interstitial sulfides.

Clearly, early precipitation and accumulation of laurite + Ru–Os–Ir alloy will have a profound effect on IPGE/PPGE fractionation, owing to the relative incompatibility of the PPGEs in both of these PGMs (Brenan and Andrews, 2001). Whether or not these phases begin to precipitate from a silicate magma will depend on the factors that control PGE solubility, which are as yet poorly constrained (see below), but certainly include fO_2 and probably fS_2 (e.g., O'Neill et al., 1995; Ertel et al., 1999; Amossé et al., 2000). An additional important factor in determining the stability of laurite and Ru–Os–Ir alloy is whether the system reaches saturation in an immiscible sulfide liquid. Early crystallization of laurite and/or Ru–Os–Ir alloy would be very effective in removing the IPGEs from the magma, thus concentrating them in the initial cumulates, and resulting in a relative enrichment of the PPGEs in the later-formed sulfide liquid. The abundances of PPGEs would thereby be controlled by the fraction of sulfide liquid present in a particular rock unit, and such relations have been well documented in the Bushveld (i.e., Maier and Barnes, 1999). For the case of sulfur-poor magmas, which never reach sulfide-liquid saturation, precipitation of laurite or Ru–Os–Ir alloy (or both) will cause IPGE-enrichment in the early-formed cumulates, with further crystallization causing progressive PPGE-enrichment in the more evolved compositions. Peck and Keays (1990) have provided a detailed account of this behavior in the Heazlewood River Complex (Tasmania), which has an abundance of Ru–Os–Ir placer deposits derived from the basal cumulates, and no associated sulfide mineralization. For magmas whose sulfur fugacities are sufficiently high that sulfide saturation occurs concurrently with the precipitation

of the primary liquidus phases, laurite + Ru–Os–Ir alloy will not form, and decoupling of the IPGE from the PPGE can only occur by crystallization of mss (e.g., Li et al., 1998), as has been documented at Sudbury (Naldrett et al., 1982; Li et al., 1992; Ballhaus et al., 2001), Noril'sk (Naldrett et al., 1994; Zientek et al., 1994) and Alexo, Ontario (Barnes and Naldrett, 1986).

6.3. Estimation of Ru activity in Ru–Os–Ir alloy

Estimation of the activity of Ru in ternary Ru–Os–Ir alloy can be made by comparing the Ru content of sulfide melt coexisting with pure Ru with that in equilibrium with Ru–Os–Ir alloy in experiments run at the same fO_2, fS_2 and temperature. In the current study, this involves comparing the result of experiments Ru3102 with RuOsIr3102A and B. Such information may be used to estimate the Ru content of silicate melt coexisting with Ru–Os–Ir alloy, given the solubility of pure Ru, which is available from the experiments of Borisov and Nachtweyh (1998). This data may, in turn, provide a more accurate evaluation of the likelihood of IPGE alloy precipitation in sulfide–undersaturated silicate melt.

At equilibrium, the activity of Ru in the sulfide melt (a_{Ru}^{melt}) is equal to that in the coexisting metal, which is unity for a melt saturated in pure Ru, i.e.:

$$a_{Ru}^{\text{sulfide melt}} = a_{Ru}^{\text{metal}} = 1. \quad (3)$$

It follows from the definition of activity that the product of the activity coefficient ($\gamma_{Ru}^{\text{sulfide melt}}$) and the mole fraction of Ru ($X_{Ru}^{\text{sulfide melt}}$) is also one, hence the activity coefficient for Ru in the sulfide melt can be calculated as:

$$\gamma_{Ru}^{\text{sulfide melt}} = 9/X_{Ru}^{\text{sulfide melt}}. \quad (4)$$

For the case of experiment Ru3102, $\gamma_{Ru}^{\text{sulfide melt}}$ is calculated to be 15.1. Assuming $\gamma_{Ru}^{\text{sulfide melt}}$ does not change significantly with $X_{Ru}^{\text{sulfide melt}}$, the activity of Ru in the ternary alloys from experiments RuOsIr3102A and B can be calculated from the expression:

$$15.1X_{Ru}^{\text{sulfide melt}} = a_{Ru}^{\text{metal}}, \quad (5)$$

which also allows the activity coefficient for Ru in the metal phase to be calculated from the expression:

$$a_{Ru}^{\text{metal}} = \gamma_{Ru}^{\text{metal}} X_{Ru}^{\text{metal}}. \quad (6)$$

The activity of Ru in the ternary alloys from experiments RuOsIr3102A ($X_{Ru}^{metal} = 0.58$) and B ($X_{Ru}^{metal} = 0.36$) are 0.24 and 0.11, respectively, which correspond to values of γ_{Ru}^{metal} equal to 0.41 and 0.30. Such values of γ_{Ru}^{metal} clearly indicate non-ideal mixing in the ternary Ru–Os–Ir system, which is not surprising, given the miscibility gaps on both the Ru–Ir and Os–Ir binary joins (Eremenko et al., 1988; Reiswig and Dickinson, 1964), which apparently extend into the Ru–Os–Ir ternary, based on compositional trends amongst natural alloys (Cabri et al., 1996).

The Ru content of silicate melt coexisting with a ternary Ru–Os–Ir alloy can be estimated by combining the alloy activity–composition relations estimated from our data with the silicate melt Ru solubility data determined by Borisov and Nachtweyh (1998). For example, at a temperature of 1300 °C and log fO_2 of −8.2 (corresponding to FMQ-1), the data of Borisov and Nachtweyh (1998) predict a Ru solubility of ~1 ppb. Assuming that the activity coefficient for Ru metal in silicate melt is independent of Ru content, the Ru concentration of a silicate melt coexisting with a ternary Ru–Os–Ir alloy will be reduced in proportion to the Ru activity in the alloy. Thus, the Ru concentration in a silicate melt coexisting with Ru–Os–Ir alloys with X_{Ru}^{metal} of 0.58 and 0.36 will be 0.24 and 0.11 ppb, respectively. An increase in fO_2 of one log unit raises the Ru solubility estimate to ~4 ppb, which corresponds to solubilities of ~2 and ~1 ppb Ru for the alloys. Such values are at or below Ru concentrations reported for sulfide-undersaturated komatiites and high Mg basalts (Brügmann et al., 1987; Puchtel and Humayun, 2000, 2001), suggesting that such magmas could be alloy saturated. We should emphasise that our estimates may be subject to considerable uncertainty, however, given that Ru solubility at low fO_2 is based on a solubility-fO_2 correlation determined at fairly oxidizing conditions (log fO_2 of −1.2 to −3). Moreover, the effect of dissolved sulfur on Ru solubility has not been determined, and could be substantial (see below), making our solubility estimates only strictly applicable to S-free magmas. In terms of the other components of Ru–Os–Ir alloys,

the solubility of pure Ir and Os metals are known to be low in molten silicate (i.e., ~ 7 ppb Ir and 40–200 ppb Os at FMQ-1; Borisov and Palme, 1995; Borisov and Walker, 2000), but activity–composition relations for these metals in such alloys are unavailable, thus an accurate estimate of the Ir and Os levels required for silicate melt saturation cannot be accurately determined at this time.

6.4. Implications for two liquid partitioning of ruthenium

At conditions of sulfide melt–silicate melt equilibrium, the activity of Ru in each phase will be the same, although the corresponding Ru concentrations may differ by orders-of-magnitude, owing to differences in the activity coefficients for these two melt types. In principle, two-liquid partition coefficients can be calculated from individual metal solubility experiments involving silicate and sulfide melts, as the activity of the metal in either melt type will be unity. We have calculated the partitioning of ruthenium between sulfide melt and host silicate magma as a function of fO_2 by ratioing our sulfide melt solubility data to values determined by Borisov and Nachtweyh (1998) for an anorthite–diopside eutectic composition. Fig. 8a portrays the Ru solubility data for the two melt types, and Fig. 8b shows the variation in calculated sulfide–silicate melt partition coefficient. As noted previously, Ru solubility in sulfide melt *decreases* slightly with increasing fO_2, while Ru solubility in the silicate melt *increases* strongly with increased fO_2. The net effect is an overall decrease in the calculated partition coefficient with increasing oxygen fugacity (Fig. 8b). Absolute values of $D_{Ru}^{sulf/sil}$ are calculated to be ~ 10^8 to ~ 10^{10} over the fO_2 range relevant to natural magmatic systems. For comparison, we have also provided in Fig. 8b a summary of sulfide–silicate melt partition coefficients for Ru that have been determined by direct measurements on equilibrated sulfide–silicate melt pairs. Regardless of fO_2, these measured values are >1000 × less than those we have calculated from metal solubility data. Below we briefly discuss the possible origins of this discrepancy, as it may offer insight into the accuracy of the available two-liquid partitioning data, and the solution properties of Ru in silicate and sulfide melts.

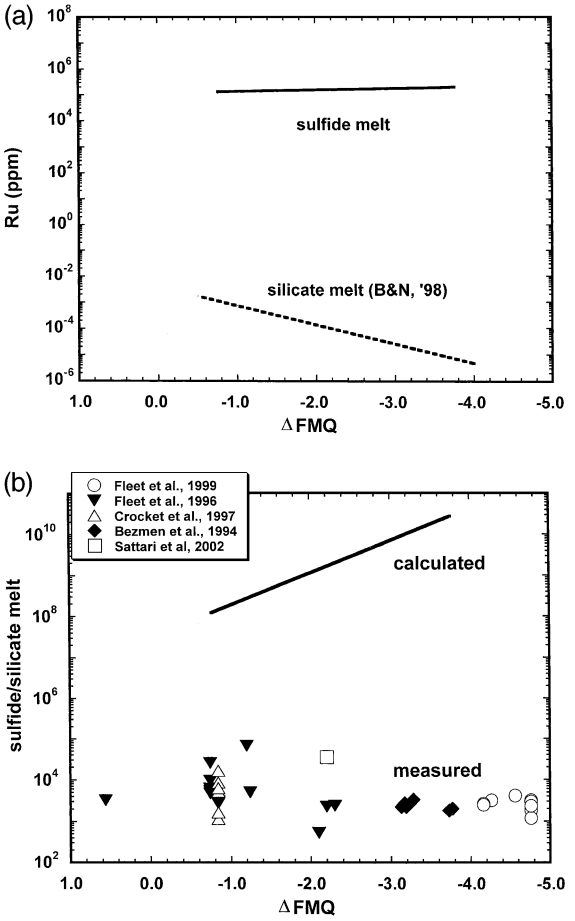

Fig. 8. (a) Plot of Ru solubility in sulfide melt (this study) and silicate melt as a function of ΔFMQ. Values for silicate melt are extrapolated from the data of Borisov and Nachtweyh (1998). (b) Plot of the calculated sulfide melt/silicate melt partition coefficient for Ru as a function of ΔFMQ based on the solubility data presented in (a). For comparison are the partition coefficients measured from experiments involving coexisting sulfide and silicate melts (sources cited: Fleet et al., 1999; Fleet et al., 1996; Crocket et al., 1997; Bezmen et al., 1994; Sattari et al., 2002).

The large discrepancy in calculated vs. measured $D_{Ru}^{sulf/sil}$ may arise from at least three sources: (1) inaccurate measurement of two-liquid partition coefficients, (2) non-Henryian solution of the PGEs in silicate melt and (3) inaccuracies in estimating Ru metal solubility in the silicate melt. In terms of the sulfide melt–silicate melt partitioning data, a common aspect of nearly all previous determinations is the use of bulk analytical techniques to determine the PGE content of mechanically separated run

products. In contrast, Sattari et al. (2002) used laser ablation ICP-MS to characterize run products from sulfide–silicate melt partitioning experiments, and observed PGE-rich spikes in the time-resolved, in situ glass analyses. Results of those experiments only yielded *minimum* two-liquid partition coefficients for Ru ($>3.5 \times 10^4$) and other PGEs, as the PGE contents of inclusion-free glass domains were below detection (<0.03 ppm Ru). As a consequence of those results, we suggest that previous partition coefficient determinations could be somewhat in error due to incomplete phase separation, as even small amounts of sulfide included in the glass phase would affect (lower) partition coefficients (see Borisov and Walker, 2000). Indeed, although Fleet et al. (1996) were able to acquire reproducible analyses on various sized glass fractions from their run products, the scale of heterogeneity observed by Sattari et al. (2002) is on the order of microns or less. It is difficult to predict, however, the exact degree to which previous results have underestimated the two-liquid partition coefficients, as the amount of included material in the glass separates from those experiments is unknown.

In terms of the solution properties of the silicate and sulfide melts, Crocket et al. (1997) documented a positive correlation between $D_{Ru}^{sulf/sil}$ and the total Ru content of the coexisting sulfide liquid, for Ru concentrations in the sulfide phase of 20–300 ppm. These results have been interpreted by Fleet et al. (1999) to correspond to non-Henryian activity composition relations in one or both of the melt phases. Thus, the large partition coefficients that we have calculated for conditions of Ru saturation in both melts would appear to be predicted by those results. A significant extrapolation of the trend depicted in Fig. 2a of Crocket et al. (1997) yields a sulfide–silicate partition coefficient of $\sim 6 \times 10^6$ at 10,000 ppm Ru in the sulfide liquid, which approaches the values we have estimated at ΔFMQ of 0.9, but still falls short by $100\times$. Thus, non-Henryian effects on two-liquid partitioning may indeed account for at least part of the discrepancy between calculated and measured values. However, as the apparent non-Henryian effects reported by Crocket et al. (1997) have only been documented over a limited concentration range, and involve significant scatter in coexisting silicate melt concentrations, better characterization of this phenomenon is certainly in order.

A final source of discrepancy in calculated vs. measured $D_{Ru}^{sulf/sil}$ is an inaccurate estimation of the Ru metal solubility in silicate melt, which may arise from at least two sources: (1) uncertainty in the low-fO_2 extrapolation of solubilities that have been measured at high fO_2 and (2) the possible effect of dissolved sulfur on enhancing metal solubilities in the silicate melt. In terms of the first effect, the Ru solubilities provided by Borisov and Nachtweyh (1998) were measured at ΔFMQ of +3 to +5, whereas conditions for basalt petrogenesis (and our calculations) are in the range of ΔFMQ of +1.5 to −2.5 (e.g., Wallace and Carmichael, 1992). The extrapolation to low solubility is based on the implicit assumption that the valence state of Ru stays constant, and thus, melt species present at high fO_2 persist into the low fO_2 regime. Ertel et al. (1999) measured Rh and Pt solubilities over a somewhat broader range of fO_2, and their results suggest that this assumption is valid for those elements. In contrast, Borisov et al. (1994) determined that the variation in Pd solubility with fO_2 reflects a change in the proportion of Pd^{2+}, Pd^{+} and Pd^{0} species such that the fO_2 dependence of Pd solubility is reduced with decreasing fO_2. If this were the case for Ru, then solubilities extrapolated from high fO_2 data could be significantly underestimated at low fO_2. Thus, "true" Ru solubilities at low fO_2 could be higher, resulting in a reduction in calculated two-liquid Ds, making our estimates more in line with direct determinations. In terms of the effect of dissolved sulfur, although O'Neill et al. (1995) argue that S should not affect the solubility of siderophile elements in silicate melt, Amossé et al. (2000) have shown that Rh, Ir and Pt solubility markedly increase with increasing fS_2. Inasmuch as the formation of an immiscible sulfide melt requires significant levels of dissolved sulfur in the silicate melt, we view this effect as potentially significant.

7. Conclusions

We have found that the solution behavior of ruthenium (and probably other PGEs) in molten sulfide is

complex, with solubility being a strong function of fO_2, fS_2, melt Fe/Ni and temperature. However, consideration of solubilities that would prevail at conditions relevant to sulfide liquid saturation in mafic magmas yields values that are uniformly high, even on dilution with other IPGEs. Such solubility levels far exceed those found even in ore-grade sulfide liquid segregations, suggesting crystallization of IPGE alloy (and laurite) in the presence of sulfide liquid is unlikely. It is thus our conclusion that if IPGE-rich PGMs are liquidus phases, the occurrence of interstitial base metal sulfide associated with rocks containing these minerals must reflect the introduction of sulfide liquid at a stage subsequent to PGM crystallization and entrapment by primary mafic phenocrysts. Hence, the timing of sulfide immiscibility is crucial if IPGE-rich phases are to crystallize and separate from mafic magmas. Based on our estimates of the activity of Ru in ternary Ru–Ir–Os alloy, it appears that Ru concentrations in silicate melt required for alloy saturation are very low (ppb to sub-ppb), which is at or below levels found in some high Mg igneous rocks. Although similar activity–composition data are as yet unavailable for Os and Ir, the overall low solubility of both these metals in silicate melt suggests alloy saturation in natural, sulfide-undersaturated systems is certainly plausible. As a final point, the sulfide melt–silicate melt partitioning we have calculated based on the solubility of Ru in each of these phases is extreme, with values of up to $\sim 10^{10}$ at very low oxygen fugacities. Such large partition coefficients could be real, and possibly reflect problems with analyzing separated run products from partitioning experiments using bulk methods. Alternatively, high values may be a consequence of non-Henryian activity–composition relations for Ru in either melt, or an artifact of our underestimating the solubility of Ru in molten silicate at the conditions relevant to saturation in immiscible sulfide liquid. In terms of the latter, possible changes in Ru valence state with decreased fO_2, or the presence of dissolved sulfur, are both likely to enhance Ru solubility in silicate melt, thus decreasing calculated two-liquid partition coefficients. In any case, it seems clear that a complete understanding of Ru solubility behaviour in molten silicate is still pending, as is likely for the other PGEs, and there is a clear need for high precision solubility measurements at low fO_2, and in the presence of dissolved sulfur.

Acknowledgements

We are grateful to Dr. L. Cabri for his interest in this work, and sharing his extensive database on PGM compositions. A. Borisov and J. Crocket offered helpful journal reviews. Experimental work at University of Toronto was funded by NSERC operating grant RGPIN 194228 to J. Brenan. Graduate student support to D. Andrews was provided through an Ontario Graduate Scholarship and a Premier's Research Excellence Award. **[RR]**

References

Amossé, J., Dable, P., Allibert, M., 2000. Thermochemical behaviour of Pt, Ir, Rh and Ru vs fO_2 and fS_2 in a basaltic melt. Implications for the differentiation and precipitation of these elements. Miner. Petrol. 68, 29–62.

Bacuta Jr., G.C., Kay, R.W., Gibbs, A.K., Lipin, B.R., 1990. Platinum group element abundance and distribution in chromite deposits of the Acoje Block, Zambales Ophiolite Complex, Philippines. J. Geochem. Explor. 37, 113–145.

Ballhaus, C., Tredoux, M., Späth, A., 2001. Phase relations in the Fe–Ni–Cu–PGE–S system at magmatic temperature and application to massive sulfide ores of the Sudbury Igneous Complex. J. Pet. 42, 1911–1926.

Barnes, S.-J., Naldrett, A.J., 1986. Variations in platinum group element concentrations in the Alexo mine komatiite, Abitibi greenstone belt, Northern Ontario. Geol. Mag. 123, 515–524.

Barnes, S.-J., Picard, C.P., 1993. The behavior of platinum group elements during partial melting, crystal fractionation, and sulfide segregation: an example from the Cape Smith Fold Belt, northern Quebec. Geochim. Cosmochim. Acta 57, 79–87.

Barnes, S.-J., Naldrett, A.J., Gorton, M.P., 1985. The origin of the fractionation of the platinum group elements in terrestrial magmas. Chem. Geol. 53, 303–323.

Bezmen, N.I., Asif, M., Brugmann, G.E., Romanenko, I.M., Naldrett, A.J., 1994. Distribution of Pd, Rh, Ru, Ir, Os, and Au between sulfide and silicate melts. Geochim. Cosmochim. Acta 58, 1251–1260.

Borisov, A., Nachtweyh, K., 1998. Ru solubility in silicate melts: experimental results in oxidizing region. Lunar and Planetary Science Conf. XXIX, 1320. Abstract.

Borisov, A., Palme, H., 1995. Solubility of iridium in silicate melts: new data from experiments with $Ir_{10}Pt_{90}$ alloys. Geochim. Cosmochim. Acta 59, 481–485.

Borisov, A., Palme, H., 2000. Solubilities of noble metals in Fe-containing silicate melts as derived from experiments in Fe-free systems. Am. Mineral. 85, 1665–1673.

Borisov, A., Walker, R.J., 2000. Os solubility in silicate melts: new efforts and results. Am. Mineral. 85, 912–917.

Borisov, A., Palme, H., Spettel, B., 1994. Solubility of palladium in

silicate melts: implications for core formation in the Earth. Geochim. Cosmochim. Acta 58, 705–716.

Brenan, J.M., Andrews, D.R., 2001. High-Temperature stability of laurite and Ru–Os–Ir alloy and their role in PGE fractionation in mafic magmas. Can. Mineral. 39, 341–360.

Brenan, J.M., Caciagli, N.C., 2000. Fe–Ni exchange between olivine and sulfide liquid: implications for oxygen barometry in sulfide-saturated magmas. Geochim. Cosmochim. Acta 64, 307–320.

Brenan, J.M., Rose, L.A., 2002. Experimental constraints on the wetting of chromite by sulfide liquid. Can. Mineral., in press.

Brügmann, G.E., Arndt, N.T., Hofmann, A.W., Tobschall, H.J., 1987. Noble metal abundances in komatiite suites from Alexo, Ontario and Gorgona Island, Colombia. Geochim. Cosmochim. Acta 51, 2159–2169.

Cabri, L.J., Harris, D.C., Weiser, T.W., 1996. The mineralogy and distribution of platinum group mineral (PGM) placer deposits of the world. Explor. Min. Geol. 5 (2), 73–167.

Carmichael, I.S.E., 1991. The redox state of basic and silicic magmas: a reflection of their source regions? Contrib. Mineral. Petrol. 106, 129–141.

Crocket, J.H., Fleet, M.E., Stone, W.E., 1997. Implications of composition for experimental partitioning of platinum group elements and gold between sulfide liquid and basalt melt: the significance of nickel content. Geochim. Cosmochim. Acta 61, 4139–4150.

Edwards, S.J., 1990. Harzburgites and refractory melts in the Lewis Hills massif, Bay of Islands ophiolite complex: the base-metals and precious-metals story. Can. Mineral. 28, 537–552.

Eremenko, V.N., Khoruzhaya, V.G., Shtepa, T.D., 1988. Temperature of nonvariant equilibria in the systems Zr–Ru and Ru–Ir. Izv. Akad. Nauk SSSR, Met. 1, 197–202. Russ. Metall. 1, 194–198, In Russian; TR.

Ertel, W., O'Neill, H.St.C., Sylvester, P.J., Dingwell, D.B., 1999. Solubilities of Pt and Rh in a haplobasaltic melt at 1300 °C. Geochim. Cosmochim. Acta 55, 245–253.

Fleet, M.E., Stone, W.E., 1991. Partitioning of platinum-group elements in the Fe–Ni–S system and their fractionation in nature. Geochim. Cosmochim. Acta 55, 345–353.

Fleet, M.E., Crocket, J.H., Stone, W.E., 1996. Partitioning of platinum group elements (Os, Ir, Ru, Pt, Pd) and gold between sulfide liquid and basalt melt. Geochim. Cosmochim. Acta 60, 2397–2412.

Fleet, M.E., Crocket, J.H., Menghua, L., Stone, W.E., 1999. Laboratory partitioning of platinum-group elements (PGE) and gold with application to magmatic sulfide-PGE deposits. Lithos 47, 127–142.

Harris, D.C., Cabri, L.J., 1973. The nomenclature of natural alloys of osmium, iridium and ruthenium based on new compositional data of alloys from world wide occurrences. Can. Mineral. 12, 104–112.

Keays, R.R., 1982. Palladium and iridium in komatiites and associated rocks: application to petrogenetic problems. In: Arndt, N.T., Nisbet, E.G. (Eds.), Komatiites. George Allen and Unwin, London, UK, pp. 435–457.

Kress, V., Carmichael, I.S.E., 1988. Stoichiometry of the iron oxidation reaction in silicate melts. Am. Mineral. 73, 1267–1274.

Legendre, O., Auge, T., 1986. Mineralogy of platinum group mineral inclusions in chromitites from different ophiolite complexes. In: Gallagher, M.J., Ixer, R.A., Neary, C.R., Prichard, H.M. (Eds.), Metallogeny of Basic and Ultrabasic Rocks. Inst. Mining Metallurgy, London, UK, pp. 361–375.

Li, C., Naldrett, A.J., Coats, C.J.C., Johannessen, P., 1992. Platinum, palladium, gold, and copper-rich stringers at the Strathcona mine, Sudbury: Their enrichment by fractionation of a sulfide liquid. Econ. Geol. 87, 1584–1598.

Li, C., Barnes, S.-J., Makovicky, E., Rose-Hansen, J., Makovicky, M., 1998. Partitioning of nickel, copper, iridium, rhenium, platinum and palladium between monosulfide solid solution and sulfide liquid: effects of composition and temperature. Geochim. Cosmochim. Acta 60, 1231–1238.

Maier, W.D., Barnes, S.-J., 1999. Platinum-group elements in silicate rocks of the lower, critical and main zones at Union Section, western Bushveld Complex. J. Petrol. 40, 1647–1671.

Maier, W.D., Prichard, H.M., Barnes, S.-J., Fisher, P.C., 1999. Compositional variation of laurite at Union Section in the Western Bushveld Complex. S. Afr. J. Geol. 102, 286–292.

Merkle, R.K.W., 1992. Platinum group minerals in the middle group of chromitite layers at Marikana, western Bushveld Complex: indicators for collection mechanisms and postmagmatic modification. Can. J. Earth Sci. 29, 209–221.

Naldrett, A.J., 1981. Platinum group element deposits. Platinum Group Elements: Mineralogy, Geology, Recovery. CIM Special, vol. 23.

Naldrett, A.J., Innes, D.G., Sowa, J., Gorton, M.P., 1982. Compositional variations within and between five Sudbury ore deposits. Econ. Geol. 77, 1519–1534.

Naldrett, A.J., Pessaran, A., Asif, M., Li, C., 1994. Compositional variation in Sudbury ores and prediction of the proximity of footwall copper-PGE orebodies. In: Lightfoot, P.C., Naldrett, A.J. (Eds.), The Sudbury Noril'sk Symposium. Ont. Geol. Sur. Spec. Pub., vol. 5, pp. 133–146.

O'Neill, H.St.C., Dingwell, D.B., Borisov, A., Spettel, B., Palme, H., 1995. Experimental petrochemistry of some highly siderophile elements at high temperatures, and some implications for core formation and the mantle's early history. Chem. Geol. 120, 255–273.

Page, N.J., Talkington, R.W., 1984. Palladium, Platinum, Rhodium, Ruthenium and Iridium in Peridotites and Chromitites from ophiolite complexes in Newfoundland. Can. Mineral. 22, 137–149.

Peach, C.L., Mathez, E.A., 1996. Constraints on the formation of platinum group element deposits in igneous rocks. Econ. Geol. 77, 1405–1418.

Peck, D.C., Keays, R.R., 1990. Insights into the behavior of precious metals in primitive, S-undersaturated magmas: evidence from the Heazlewood River Complex, Tasmania. Can. Mineral. 28, 373–387.

Peck, D.C., Keays, R.R., Ford, R.J., 1992. Direct crystallization of refractory platinum group elements alloys from boninitic magmas: evidence from western Tasmania. Aust. J. Earth Sci. 39, 373–387.

Pownceby, M.I., O'Neill, H.St.C., 1994. Thermodynamic data from redox reactions at high temperatures. III. Activity–composition relations in Ni–Pd alloys from EMF measurements at 850–1250 K, and calibration of the NiO+Ni–Pd assemblage as a redox sensor. Contrib. Mineral. Petrol. 116, 327–339.

Prichard, H.M., Neary, C.R., Potts, P.J., 1986. Platinum group minerals in the Shetland ophiolite. Metallogeny of Basic and Ultra basic Rocks. Inst. of Mining Metall. London, UK, pp. 395–414.

Puchtel, I., Humayun, M., 2000. Platinum group elements in Kostomuksha komatiites and basalts: implications for oceanic crust recycling and core–mantle interaction. Geochim. Cosmochim. Acta 64, 4227–4242.

Puchtel, I., Humayun, M., 2001. Platinum group element fractionation in a komatiitic basalt lava lake. Geochim. Cosmochim. Acta 65, 2979–2994.

Reiswig, R.D., Dickinson, J.M., 1964. Trans. AIME 230 (4), 469–472.

Robie, R.A., Hemingway, B.S., Fisher, J.R., 1979. Thermodynamic properties of minerals and related substances at 298.15 K and 1 bar (105 Pascals) pressure and at higher temperature. USGS Bull., 1452.

Rose, L.A., Brenan, J.M., 2001. Wetting Properties of Fe–Ni–Co–Cu–O–S Melts against Olivine: Implications for Sulfide Melt Mobility. Econ. Geol. 96, 145–157.

Sattari, P., Brenan, J.M., Horn, I., McDonough, W.F., 2002. Experimental constraints on the sulfide– and chromite–silicate melt partitioning behavior of rhenium and the platinum group elements. Econ. Geol. 97, 385–398.

Snyder, D.A., Carmicheal, I.S.E., 1992. Olivine-liquid equilibria and the chemical activities of FeO, NiO, Fe_2O_3, and MgO in natural basic melts. Geochim. Cosmochim. Acta 56, 303–318.

Talkington, R.W., Lipin, B.R., 1986. Platinum group minerals in chromite seams of the Stillwater Complex, Montana. Econ. Geol. 81, 1179–1186.

Torres-Ruiz, J., Garuti, G., Gazzotti, M., Gervilla, F., Fenoll Hach-Ali, P., 1996. Platinum group minerals in chromitites from the Ojen lherzolite massif (Serrania de Ronda, Beltic Cordillera, Southern Spain). Mineral. Petrol. 56, 25–50.

Toulmin III., P., Barton Jr., P.B., 1964. A thermodynamic study of pyrite and pyrrhotite. Geochim. Cosmochim. Acta 28, 641–671.

von Gruenewaldt, G., Hulbert, L.J., Naldrett, A.J., 1989. Contrasting platinum group element concentration patterns in cumulates of the Bushveld Complex. Mineral. Dep. 24, 219–229.

Wallace, P., Carmichael, I.S.E., 1992. Sulphur in basaltic magmas. Geochim. Cosmochim. Acta 56, 1863–1874.

Watson, B.E., 1981. Melt infiltration and magma evolution. Geology 10, 236–240.

Zientek, M.L., Likhachev, A.P., Kunilov, V.E., Barnes, S.-J., Meier, A.L., Carlson, R.R., Briggs, P.H., Fries, T.L., Adrian, B.M., 1994. Cumulus processes and the composition of magmatic ore deposits: examples from the Talnakh district, Russia. In: Lightfoot, P.C., Naldrett, A.J. (Eds.), The Sudbury Noril'sk Symposium. Ont. Geol. Sur. Spec. Pub., vol. 5, pp. 133–146.